Geochemical Perspectives Letters

Ancient mantle plume components constrained by tungsten isotope variability in arc lavas

N. Messling, G. Wörner, M. Willbold

Supplementary Information

The Supplementary Information includes:

- Methods
- Binary Mixing Models
- Supplementary Tables S-1 to S-5
- Supplementary Figures S-1 to S-5
- Supplementary Information References

Methods

Analytical techniques utilised in this study are based on W separation procedures described in earlier work (Willbold *et al.*, 2011; Mei *et al.*, 2018; Tusch *et al.*, 2019). We further optimised the W separation procedure for larger sample sizes while maintaining measurement precision and accuracy. Therefore, we devised a new W separation procedure to process up to 6 g of sample material on a three-step ion exchange chromatography. We utilised the precipitation of a W-free fluoride phase during sample digestion, which removed the majority of matrix elements, while quantitatively retaining W. Sample preparation was carried out under metal-free clean laboratory conditions at the University of Göttingen.

1. Sample preparation and trace element measurement

All adakites and basanites were available as powders that were initially used by Abratis and Wörner (2001) and Wegner *et al.* (2011). These powders were prepared using an agate ball mill after crushing in the field and washing with distilled water. Additional samples from accreted fore-arc terranes (QUE-020, PAR-023 and PAV-030) were crushed into 1–2 cm large chips in a steel jaw crusher. To avoid metal contamination the samples were then washed with Milli-Q water (Merck Millipore). After drying, the chips were packed into plastic bags and crushed with a hydraulic press into pieces smaller than 5 mm. The crushed samples were ground in agate ball mills and used for trace element and isotopic analysis. The new trace element measurements were conducted as described in Hegner *et al*. (2022) on a ThermoFisher Scientific iCap Q-ICPMS. Sample powders were digested in a picotrace DAS high-pressure digestion system at 220 °C in 1.2 mL concentrated HF and 0.3 mL concentrated HNO_3 to ensure complete digestion of refractory minerals. In addition, reference materials ranging from basalts to rhyolites were equally prepared in order to accurately represent the compositional range of samples measured in this study.

2. Tungsten sample digestion and separation

All steps were carried out using double distilled acids (Savillex DST-1000) or ultra-pure reagents, which were diluted to appropriate concentrations using 18.2 MΩ cm water (Merck Millipore Milli-Q). Between 2 and 6 g of sample powder were weighed out in 60 or 90 mL Savillex beakers. For every 2 g of sample powder, 10 mL 6 M HCl and 10 mL 24 M HF were added. In the closed beaker the samples were digested at 150 °C for 3 days, ultrasonicating the samples at the beginning and end of the digestion. After completely drying down the sample at 130 °C, 10 mL 0.5 M HCl–1 M HF were added and heated for 1–2 h. The samples were transferred into a 50 mL centrifuge tube and centrifuged for 15 min. The acid supernatant was decanted and stored in another centrifuge tube. To the fluoride residue, another 10 mL 0.5 M HCl–1 M HF were added, which was then placed into a heated ultrasonic bath at 60 °C for 15 min. After centrifuging and decanting this step was repeated once more. W was quantitively transferred into the supernatant at this point (Fig. S-3a). The fluoride residue, containing a significant fraction of matrix elements was therefore discarded. The 30 mL of the combined supernatant were used for the ion exchange procedure. The full elution scheme of all ion exchange procedures used is described in Table S-2. After the first anion (10 mL AG1x8) chemistry the sample solution was directly passed through an Eichrom prefilter column to remove dissolved organic compounds. After this step and every following ion exchange chromatography samples were treated with HNO_3–H_2O_2 as described in Tusch *et al.* (2019). On the following 1 mL TEVA column, W was separated from the remaining HFSE as described in Mei *et al.* (2018). Lastly, a 1 mL anion clean-up chemistry was used to separate remaining matrix elements. For several samples, an aliquot was taken after the digestion of the samples to show no W is lost during the fluoride precipitation procedure. Typically, 60–90 % of the W budget of the samples is recovered using this chemical separation procedure (Fig. S-3b). Further, we compared digestion yields of the reference material JB-2 for complete digestion and fluoride precipitation digestion. All results are provided in Figure S-3a. Procedural blanks for the entire chemical separation procedure ranged from 96 to 841 pg for every 6 g of digested material, with an average of 346 pg (n = 9) corresponding to an average blank contribution of 0.6 ‰. Elution patterns for the first anion and the TEVA exchange chromatography for some matrix elements and the HFSE is provided in Figure S-4.

3. Tungsten isotope measurement

The W isotopic compositions of samples and reference materials were determined on a Thermo Fisher Scientific Neptune Plus MC-ICP-MS at the University of Göttingen. A Teledyne Cetac Aridus III desolvating nebuliser equipped with the Teledyne Cetac QuickWash3 accessory was used as the sample introduction system. Similar to Tusch *et al.* (2019), a cyclonic quartz spray chamber was interconnected between the desolvating nebuliser and the torch to improve the signal stability by increasing the expansion volume of the inlet system. Faraday cups were connected to a series of 10^{11}, 10^{12} and 10^{13} Ω amplifier boards to measure ion currents of the W isotopes, as well as those of ^{177}Hf, ^{178}Hf, ^{181}Ta and ^{188}Os, which were monitored for the correction of isobaric interferences on W. 10^{11} Ω amplifiers were used for ^{177}Hf, ^{182}W, ^{183}W, ^{184}W and ^{186}W, whereas ^{188}Os was monitored using a 10^{12} Ω amplifier and ^{178}Hf and ^{180}W using a 10^{13} Ω amplifier. Typical sensitivities with a Ni standard sample cone and X skimmer cone and a 60 µL/min nebuliser were 300–350 V/ppm of total W. Triplet analyses were conducted for each sample, with 60 cycles and an integration time of 8.39 seconds per analysis. For samples with high W concentrations 6 individual measurements were conducted. Each sample was bracketed with a 240 ng/g W NIST SRM 3163 solution. Data reduction was carried out offline using a Python script using exponential law to correct for mass bias, normalising to $^{186}W/^{184}W$ = 0.92767 (Völkening *et al.*, 1991). For a high-precision triplet measurement, ~650 ng of W were required. The external reproducibility was calculated by repeated measurements of in-house reference materials ‘Granite 232’ (described in Haack, 1969) and ‘Basalt Me21’, collected from the ‘Hoher Meißner’ basalt quarry, that were measured at the beginning and the end of every measurement sequence (Fig. S-5). Data is expressed as $\mu^{182}W$ which is defined as $(^{182}W/^{184}W_{sample} / {}^{182}W/^{184}W_{NIST\ 3163} - 1) \times 1{,}000{,}000$. The external $\mu^{182}W$

reproducibility (2 s.d.) for Granite 232 is 3.61 ppm (n = 13) and 4.36 ppm for Me21 (n = 24) for triplet measurements. For sextuplet analysis, the reproducibility was improved to 2.95 ppm for Me21 (n = 8), in good agreement with the external reproducibility reported in recent literature (2.9–4.5 ppm, Jansen *et al.*, 2022; 1.45–2.73 ppm, Tusch *et al.*, 2022). The W isotope data for single measurements is provided in Figure S-4 together with $\mu^{183}W$ data and values normalised to $^{186}W/^{183}W$. This also includes $\mu^{182}W$ values (normalised to $^{186}W/^{183}W$), corrected for mass-independent fractionation with the equation from Budde *et al.* (2022). We observe mass-independent W isotope variations resulting in deficits in $\mu^{182}W$ as low as -20 ppm, similar to previous studies (Kruijer and Kleine, 2018; Archer *et al.*, 2019; Tusch *et al.*, 2019; Tappe *et al.*, 2020; Budde *et al.*, 2022). This effect likely occurs during the dry-down procedure between ion exchange chromatography steps and often coincides with significant losses of W (Willbold *et al.*, 2011; Tusch *et al.*, 2019; Budde *et al.*, 2022). We applied the dry-down procedure described by Tusch *et al.* (2019), adding several steps of HNO_3–H_2O_2 to the W cuts following the dry-down after each chromatography step. However, this procedure does not result in a decrease in the ^{183}W effect in our samples. The precipitation of fluorides likely has no influence on the analytical ^{183}W effect, since the magnitude of this effect is in line with previous methods that applied a complete digestion procedure (Tusch *et al.*, 2019). In this study, we used $^{186}W/^{184}W$ for the mass bias correction to avoid any analytical effects of ^{183}W. When corrected for mass-independent fractionation (Budde *et al.*, 2022), $\mu^{182}W$ values normalised to $^{186}W/^{183}W$ are in good agreement with those normalised to $^{186}W/^{184}W$ within 3 ppm (Table S-4).

Binary Mixing Models

The models shown in Figures 2 and 3 are based on simple binary mixing calculations between a mantle wedge with a depleted mantle or enriched mantle composition. All parameters relevant for modelling are summarised in Table S-3. In the model, we assume a slab melt composition that was produced by partially melting a protolith with a composition of the average CCR basalts and a residual eclogitic mineral assemblage from Gazel *et al.* (2009). We calculated the HFSE abundances in the slab melt using partition coefficients from Kessel *et al.* (2005). We did not use Nb/La ratios reported in Gazel *et al.* (2009), since these were higher than the Nb/La ratios measured in the adakites. Partition coefficients for W between melt and rutile during slab melting are poorly constrained. The W/Th ratio was therefore estimated based on the lowest W/Th ratio of the adakites (W/Th = 0.023) as well as their major element chemistry (SiO_2 = 53 to 69 wt. %). For instance, assuming a slab melt W/Th ratio >0.019 would require a 35 % contribution from the slab melt, resulting in an unrealistically high SiO_2 (>57 wt. %) content in the hybridised bulk mantle composition. On the other end of the spectrum, assuming a W/Th ratio <0.014 for the slab melt, a W isotope deficit exceeding the composition of basalts from the modern central Galápagos domain ($\mu^{182}W > -22$) would be necessary to achieve the measured W isotopic composition of the adakites with this model. The currently subducting Cocos and Coiba ridges fully reflect the chemical zonation of the Galápagos Archipelago (*e.g.*, Werner *et al.*, 2003). It is therefore unlikely that the W isotopic composition of the subducted ridges only represent the central Galápagos domain. As such, we assume an intermediary W/Th ratio of 0.018 in our model, yielding slab melt contributions of 3 to 20 % that are in good agreement with radiogenic isotope modelling from Gazel *et al.* (2009). As a result, the slab melt components in the central American arc system only require a $\mu^{182}W$ isotope composition of 0 to −12. This range is in line with the isotopic composition of accreted OIB terranes measured in this study as well as basalts from the Galápagos Archipelago. The $\mu^{182}W$ value of the upper mantle is assumed to be 0 (*e.g.*, Willbold *et al.*, 2011; Jansen *et al.*, 2022). To estimate an error for this value we used the reproducibility of our standard (95 % confidence interval: $\mu^{182}W$ = 0.98) in our model calculations. Addition of sediment can potentially provide significant contributions to the W budget in arc melts. Trace element systematics in Central American arc rock generally show decreasing sediment addition towards the

southeast (Leeman *et al.*, 1994; Patino *et al.*, 2000). In southern Costa Rica and Panama, sediment contribution to arc rocks is considered small (Bekaert *et al.*, 2021). Previous models assumed a contribution of 0.1 to 0.6 % sediment-derived melts for arc rocks in this region (Gazel *et al.*, 2009). The 'global subducted sediment' (GLOSS) composite by Plank and Langmuir (1998) does not report concentration data for W. We therefore used a W/Th ratio of 0.21 based on global W sediment data (Kirchenbaur and Münker, 2015; Kurzweil *et al.*, 2019; Stubbs *et al.*, 2022) to calculate the W concentration in the sediment melt. This likely overestimates the W contribution of sediments, as residual rutile in the sediments during subduction would result in lower W/Th ratios in the melt. However, using the maximum W/Th ratios calculated here for sediment melts and the sediment proportions estimated in Gazel *et al.* (2009), the maximum contribution of sediment melt to the average W budget of adakites is less than 4 % (<13.5 ng/g). We used the lower bound of 0.1 % sediment proportion for our calculations. Based on the model of influx and arc parallel mantle flow beneath Costa Rica and Panama (Abratis and Wörner, 2001; Hoernle *et al.*, 2008) it is reasonable to assume that the mantle wedge has been modified by subduction zone processes. To account for this, we used upper mantle W concentration of 10 ng/g for the mantle source with slightly elevated W/Th ratios of 0.19 similar to the average arc basalt (König *et al.*, 2008, 2011; Mazza *et al.*, 2020; Stubbs *et al.*, 2022). The trace element budget of the enriched Galápagos mantle source was back-calculated using the average Galápagos basalt composition compiled from the GEOROC database, while assuming 11 % batch melting of the Galápagos mantle (White *et al.*, 1993). We assumed a constant W/Th of 0.11 in agreement with W/Th ratios measured in accreted Galápagos OIB terranes as well as global OIB data (König *et al.*, 2011; Kurzweil *et al.*, 2019).

Supplementary Tables

Table S-1 W isotope and long-lived radiogenic isotope data and trace element data for reanalysed samples.

Tables S-1 (.xlsx) is available for download from the online version of this article at https://doi.org/10.7185/geochemlet.2321.

Table S-2 Tungsten ion exchange matrix separation procedure.

Step	Reagent	Acid volume (mL)
I. BioRad AG1x8 100–200 mesh, 10 mL resin (20 mL Bio-Rad Econo-Pac® columns)		
Clean	1 mM DTPA–1 M HCl	4 × 10
	3 M HNO_3–0.2 M HF	4 × 10
	6 M HNO_3–0.2 M HF	4 × 10
	H_2O	4 × 10
Condition	0.5 M HCl–1 M HF	4 × 10
Load	0.5 M HCl–1 M HF	3 × 10
Elute Matrix	0.005 M HCl–1 M HF	4 × 10
Elute HFSE and Ti	0.5 M HCl–1 % H_2O_2	10 × 10
	0.005 M HCl–1 M HF	1 × 10
Collect Mo, W, Sn	3 M HNO_3–0.2 M HF	5.5 × 10

Table S-2 continued.

Step	Reagent	Acid volume (mL)
II. Eichrom prefilter resin 100–150 mesh, 1 mL resin (2 mL Biorad Poly-Prep® columns)		
Clean	3 M HCl–0.2 M HF	2 × 10
	6 M HNO_3–0.2 M HF	2 × 10
	H_2O	1 × 10
Condition	3 M HNO_3–0.2 M HF	2 × 2
Load & Collect	3 M HNO_3–0.2 M HF	55
Collect	3 M HNO_3–0.2 M HF	2 × 1
III. Eichrom TEVA 100–150 mesh, 1 mL resin (2 mL Biorad Poly-Prep® columns) on 0.4 mL Eichrom prefilter resin		
Clean	6 M HNO_3–0.2 M HF	2 × 10
	H_2O	1 × 10
	3 M HCl–0.02 M HF	2 × 10
Condition	9 M HCl–0.02 M HF	4 × 1
Load	9 M HCl–0.02 M HF	2
Rinse	9 M HCl–0.02 M HF	5 × 0.5
Collect W	3 M HCl–0.02 M HF	4 × 2
Collect Mo	3 M HNO_3–0.2 M HF	3 × 2
IV. BioRad AG1x8 100–200 mesh, 1 mL resin (2 mL Biorad Poly-Prep® columns) on 0.4 mL Eichrom prefilter resin		
Clean	0.5 M HCl–1 M HF	1 × 10
	3 M HNO_3–0.2 M HF	1 × 10
	6 M HNO_3–0.2 M HF	1 × 10
	H_2O	2 × 2
Condition	0.5 M HCl–1 M HF	4 × 1
Load	0.5 M HCl–1 M HF	3
Elute Matrix	0.005 M HCl–1 M HF	3 × 1
Collect W	3 M HNO_3–0.2 M HF	3 × 2

Table S-3 Parameters used for the binary mixing models.

Parameter	CCR slab melt	Sediment melt	Mantle wedge	Enriched mantle	Galápagos mantle
W (ng/g)	112	2250	10	14	14[e]
W/Th	0.018	0.21[c,d]	0.19	0.11[b,c]	0.11
Nb/La	0.16	0.16[a]	0.9[f]	1.3[c]	1.4[e]
$\mu^{182}W$	0 to −12	0	0	0	0 to −6

[a] Gazel *et al*. (2009).
[b] König *et al*. (2011).
[c] Kurzweil *et al*. (2019).
[d] Kirchenbaur and Münker (2015); Stubbs *et al*. (2022).
[e] Calculated from basalt data compiled from https://georoc.eu on 22 November 2022 (Geist *et al.*, 2002, 2005, 2006; Gibson and Geist, 2010; Gibson *et al.*, 2012, 2016; Handley *et al.*, 2011; Harpp and Weis, 2020; Harpp *et al.*, 2003; Peterson *et al.*, 2017, 2014).
[f] Salters and Stracke (2004).

Table S-4 W isotope data for single measurements of samples and in-house reference materials, including values normalised to $^{186}W/^{184}W$ and $^{186}W/^{183}W$.

Table S-5 Trace element concentrations of the acid supernatant from reference material JB-2 after the fluoride leaching procedure.

Tables S-4 and S-5 (.xlsx) are available for download from the online version of this article at https://doi.org/10.7185/geochemlet.2321.

Supplementary Figures

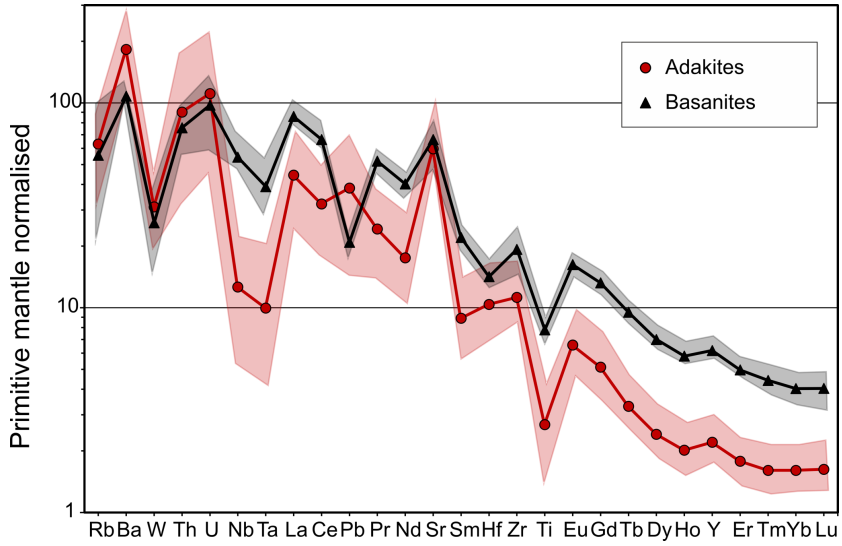

Figure S-1 Primitive mantle-normalised trace element patterns for average concentrations of adakites and basanites analysed for W isotopes. Shaded areas represent the entire trace element variability of each group. Primitive mantle values from Palme and O'Neill (2014).

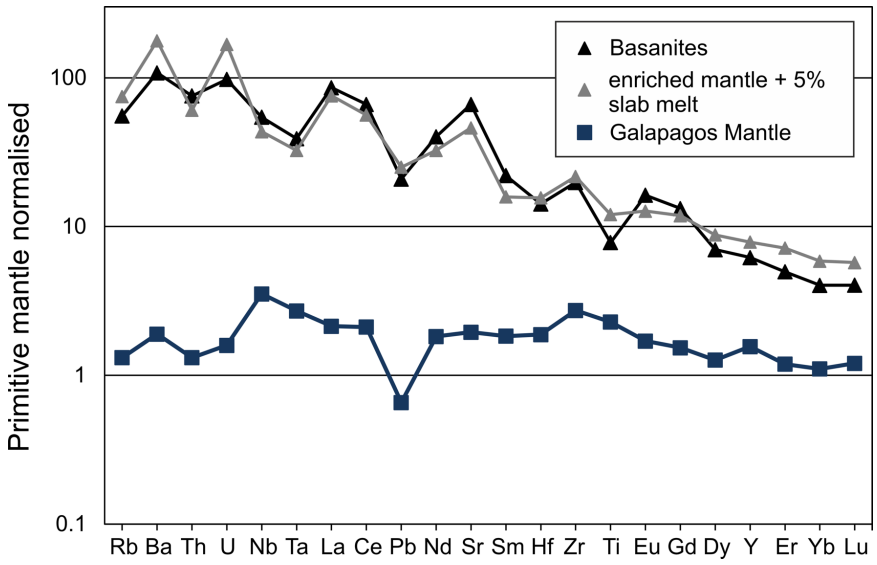

Figure S-2 Primitive mantle-normalised trace element patterns of average measured basanites plotted together with the modelled basanite melt composition. The model calculation assumes low degree melting of an enriched mantle source modified by 5 % slab melt as constrained by the modelled Nb/La and W/Th ratios shown in Figure 2. Also shown is the modelled composition of the Galápagos mantle assuming that the average Galápagos basalt was derived by 11 % batch melting of the mantle source. See text for further explanation. Primitive mantle values from Palme and O'Neill (2014).

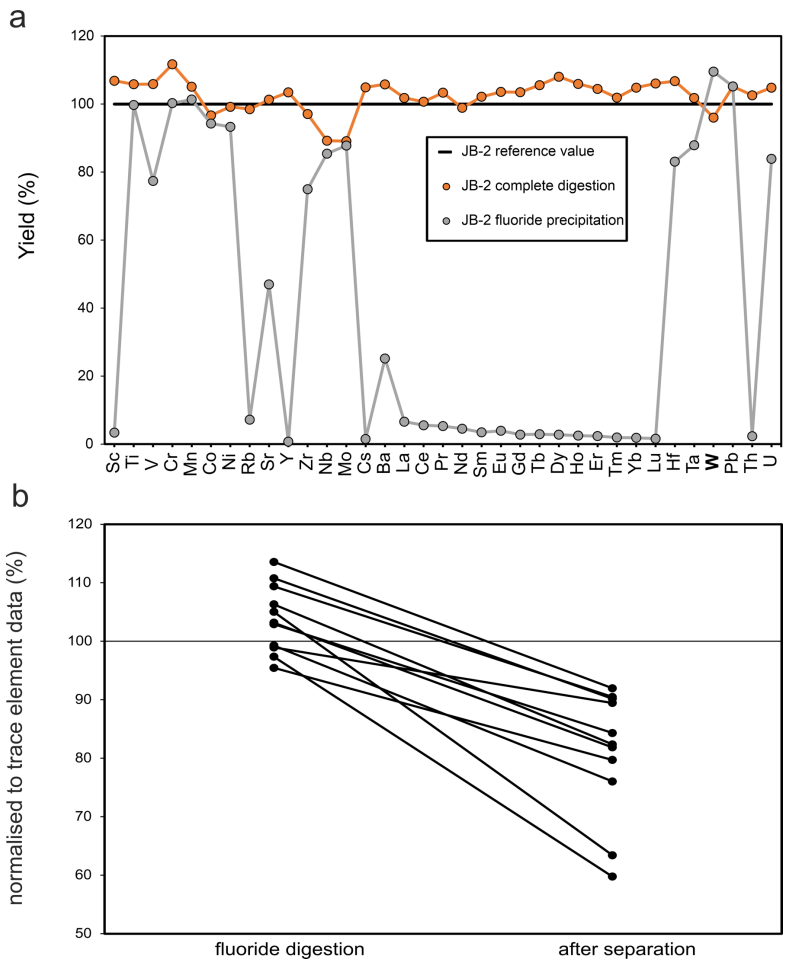

Figure S-3 **(a)** Chemistry yield of different digestion methods for selected trace elements. The fluoride-precipitation digestion was prepared under the same conditions as samples analysed for W isotopes. Normalisation values are the compiled values from for GSJ basaltic reference material JB-2 from Jochum *et al.* (2016). Trace element concentration data provided in Table S-5. **(b)** Chemistry yield from W separation procedure determined from 1 ‰ aliquots taken after sample digestion and after the separation procedure on selected samples.

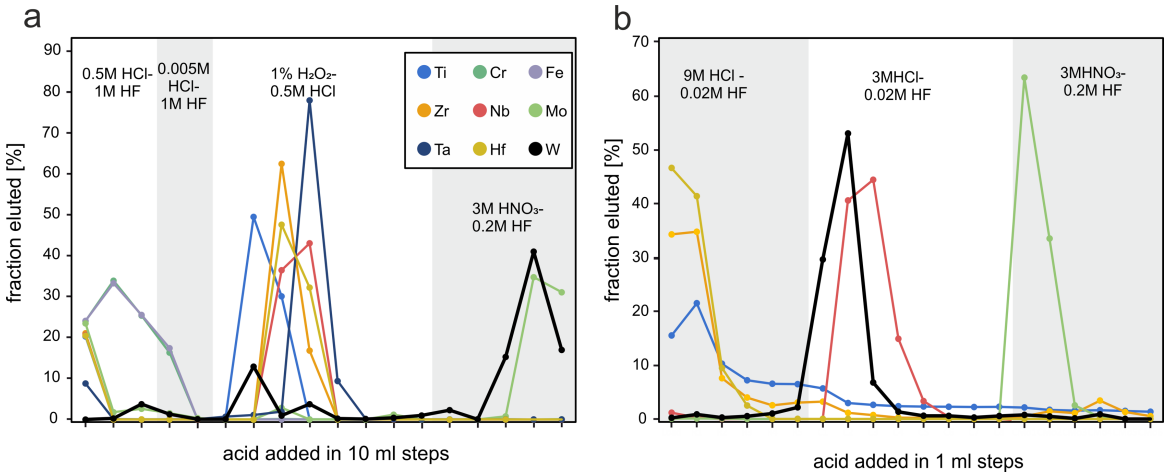

Figure S-4 Elution curves of selected elements for matrix separation procedures described in Table S-2. **(a)** I. Anion exchange chemistry (BioRad AG1x8 100–200 mesh, 10 mL resin). **(b)** III. TEVA chemistry **(**Eichrom TEVA 100–150 mesh, 1 mL resin).

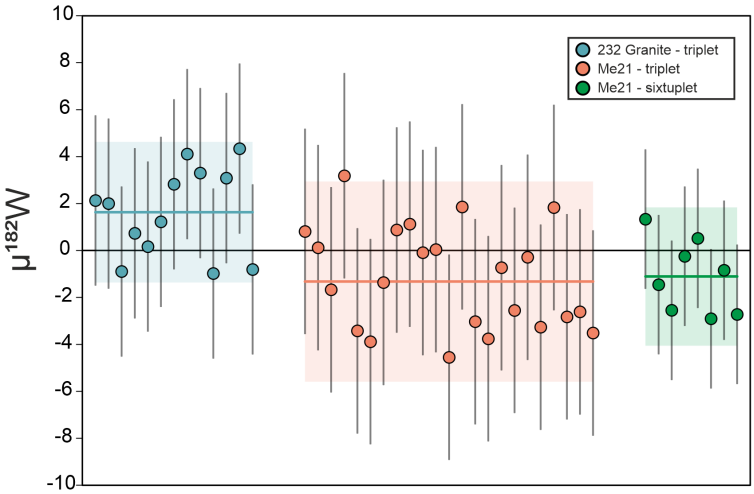

Figure S-5 $\mu^{182}W$ values of in-house reference materials Granite 232 and Me21 basalt measured over the course of two years. Coloured lines show average values of the samples. Lightly coloured areas mark the 2 s.d. calculated for each sample or method.

Supplementary Information References

Abratis, M. (1998) *Geochemical variations in magmatic rocks from southern Costa Rica as a consequence of Cocos Ridge subduction and uplift of the Cordillera de Talamanca*. PhD thesis, Universität Göttingen. http://hdl.handle.net/11858/00-1735-0000-0006-B338-3

Abratis, M., Wörner, G. (2001) Ridge collision, slab-window formation, and the flux of Pacific asthenosphere into the Caribbean realm. *Geology* 29, 127–130. https://doi.org/10.1130/0091-7613(2001)029<0127:RCSWFA>2.0.CO;2

Appel, H., Wörner, G., Alvarado, G., Rundle, C., Kussmaul, S. (1994) Age relations in igneous rocks from Costa Rica. *Profil* 7, 63–69.

Archer, G.J., Brennecka, G.A., Gleißner, P., Stracke, A., Becker, H., Kleine, T. (2019) Lack of late-accreted material as the origin of ^{182}W excesses in the Archean mantle: Evidence from the Pilbara Craton, Western Australia. *Earth and Planetary Science Letters* 528, 115841. https://doi.org/10.1016/j.epsl.2019.115841

Bekaert, D.V., Gazel, E., Turner, S., Behn, M.D., de Moor, J.M., *et al.* (2021) High ^{3}He/^{4}He in central Panama reveals a distal connection to the Galápagos plume. *Proceedings of the National Academy of Sciences* 118, e2110997118. https://doi.org/10.1073/pnas.2110997118

Budde, G., Archer, G.J., Tissot, F.L.H., Tappe, S., Kleine, T. (2022) Origin of the analytical ^{183}W effect and its implications for tungsten isotope analyses. *Journal of Analytical Atomic Spectrometry* 37, 2005–2021. https://doi.org/10.1039/D2JA00102K

Gazel, E., Carr, M.J., Hoernle, K., Feigenson, M.D., Szymanski, D., Hauff, F., van de Bogaard, P. (2009) Galapagos-OIB signature in southern Central America: Mantle refertilization by arc–hot spot interaction. *Geochemistry, Geophysics, Geosystems* 10, Q02S11. https://doi.org/10.1029/2008GC002246

Geist, D., White, W.M., Albarede, F., Harpp, K., Reynolds, R., Blichert-Toft, J., Kurz, M.D. (2002) Volcanic evolution in the Galápagos: The dissected shield of Volcan Ecuador. *Geochemistry, Geophysics, Geosystems* 3, 1061. https://doi.org/10.1029/2002GC000355

Geist, D.J., Naumann, T.R., Standish, J.J., Kurz, M.D., Harpp, K.S., White, W.M., Fornari, D.J. (2005) Wolf Volcano, Galápagos Archipelago: Melting and Magmatic Evolution at the Margins of a Mantle Plume. *Journal of Petrology* 46, 2197–2224. https://doi.org/10.1093/petrology/egi052

Geist, D.J., Fornari, D.J., Kurz, M.D., Harpp, K.S., Soule, S.A., Perfit, M.R., Koleszar, A.M. (2006) Submarine Fernandina: Magmatism at the leading edge of the Galápagos hot spot. *Geochemistry, Geophysics, Geosystems* 7, Q12007. https://doi.org/10.1029/2006GC001290

Gibson, S.A., Geist, D. (2010) Geochemical and geophysical estimates of lithospheric thickness variation beneath Galápagos. *Earth and Planetary Science Letters* 300, 275–286. https://doi.org/10.1016/j.epsl.2010.10.002

Gibson, S.A., Geist, D.G., Day, J.A., Dale, C.W. (2012) Short wavelength heterogeneity in the Galápagos plume: Evidence from compositionally diverse basalts on Isla Santiago. *Geochemistry, Geophysics, Geosystems* 13, Q09007. https://doi.org/10.1029/2012GC004244

Gibson, S.A., Dale, C.W., Geist, D.J., Day, J.A., Brügmann, G., Harpp, K.S. (2016) The influence of melt flux and crustal processing on Re–Os isotope systematics of ocean island basalts: Constraints from Galápagos. *Earth and Planetary Science Letters* 449, 345–359. https://doi.org/10.1016/j.epsl.2016.05.021

Haack, U.K. (1969) Spurenelemente in Biotiten aus Graniten und Gneisen. *Contributions to Mineralogy and Petrology* 22, 83–126. https://doi.org/10.1007/BF00372399

Hegner, E., Alexeiev, D.V, Messling, N., Tolmacheva, T.Yu., Willbold, M. (2022) Cambrian-Ordovician mid-ocean ridge magmatism in the Kyrgyz Middle Tianshan and origin of the Karaterek ophiolite. *Lithos* 410–411, 106576. https://doi.org/10.1016/j.lithos.2021.106576

Handley, H.K., Turner, S., Berlo, K., Beier, C., Saal, A.E. (2011) Insights into the Galápagos plume from uranium-series isotopes of recently erupted basalts. *Geochemistry, Geophysics, Geosystems* 12, Q0AC14. https://doi.org/10.1029/2011GC003676

Harpp, K.S., Weis, D. (2020) Insights Into the Origins and Compositions of Mantle Plumes: A Comparison of Galápagos and Hawai'i. *Geochemistry, Geophysics, Geosystems* 21, e2019GC008887. https://doi.org/10.1029/2019GC008887

Harpp, K.S., Fornari, D.J., Geist, D.J., Kurz, M.D. (2003) Genovesa Submarine Ridge: A manifestation of plume-ridge interaction in the northern Galápagos Islands. *Geochemistry, Geophysics, Geosystems* 4, 8511. https://doi.org/10.1029/2003GC000531

Hoernle, K., Abt, D.L., Fischer, K.M., Nichols, H., Hauff, F., *et al.* (2008) Arc-parallel flow in the mantle wedge beneath Costa Rica and Nicaragua. *Nature* 451, 1094–1097. https://doi.org/10.1038/nature06550

Jansen, M.W., Tusch, J., Münker, C., Bragagni, A., Avanzinelli, R., Mastroianni, F., Stuart, F.M., Kurzweil, F. (2022) Upper mantle control on the W isotope record of shallow level plume and intraplate volcanic settings. *Earth and Planetary Science Letters* 585, 117507. https://doi.org/10.1016/j.epsl.2022.117507

Jochum, K.P., Weis, U., Schwager, B., Stoll, B., Wilson, S.A., Haug, G.H., Andreae, M.O., Enzweiler, J. (2016) Reference Values Following ISO Guidelines for Frequently Requested Rock Reference Materials. *Geostandards and Geoanalytical Research* 40, 333–350. https://doi.org/10.1111/j.1751-908X.2015.00392.x

Kessel, R., Schmidt, M.W., Ulmer, P., Pettke, T. (2005) Trace element signature of subduction-zone fluids, melts and supercritical liquids at 120–180 km depth. *Nature* 437, 724–727. https://doi.org/10.1038/nature03971

Kirchenbaur, M., Münker, C. (2015) The behaviour of the extended HFSE group (Nb, Ta, Zr, Hf, W, Mo) during the petrogenesis of mafic K-rich lavas: The Eastern Mediterranean case. *Geochimica et Cosmochimica Acta* 165, 178–199. https://doi.org/10.1016/j.gca.2015.05.030

König, S., Münker, C., Schuth, S., Garbe-Schönberg, D. (2008) Mobility of tungsten in subduction zones. *Earth and Planetary Science Letters* 274, 82–92. https://doi.org/10.1016/j.epsl.2008.07.002

König, S., Münker, C., Hohl, S., Paulick, H., Barth, A.R., Lagos, M., Pfänder, J., Büchl, A. (2011) The Earth's tungsten budget during mantle melting and crust formation. *Geochimica et Cosmochimica Acta* 75, 2119–2136. https://doi.org/10.1016/j.gca.2011.01.031

Kruijer, T.S., Kleine, T. (2018) No ^{182}W excess in the Ontong Java Plateau source. *Chemical Geology* 485, 24–31. https://doi.org/10.1016/j.chemgeo.2018.03.024

Kurzweil, F., Münker, C., Grupp, M., Braukmüller, N., Fechtner, L., Christian, M., Hohl, S.V., Schoenberg, R. (2019) The stable tungsten isotope composition of modern igneous reservoirs. *Geochimica et Cosmochimica Acta* 251, 176–191. https://doi.org/10.1016/j.gca.2019.02.025

Leeman, W.P., Carr, M.J., Morris, J.D. (1994) Boron geochemistry of the Central American Volcanic Arc: Constraints on the genesis of subduction-related magmas. *Geochimica et Cosmochimica Acta* 58, 149–168. https://doi.org/10.1016/0016-7037(94)90453-7

Mazza, S.E., Stracke, A., Gill, J.B., Kimura, J.-I., Kleine, T. (2020) Tracing dehydration and melting of the subducted slab with tungsten isotopes in arc lavas. *Earth and Planetary Science Letters* 530, 115942. https://doi.org/10.1016/j.epsl.2019.115942

Mei, Q.-F., Yang, J.-H., Yang, Y.-H. (2018) An improved extraction chromatographic purification of tungsten from a silicate matrix for high precision isotopic measurements using MC-ICPMS. *Journal of Analytical Atomic Spectrometry* 33, 569–577. https://doi.org/10.1039/C8JA00024G

Palme, H., O'Neill, H.St.C. (2014) 3.1 - Cosmochemical Estimates of Mantle Composition. In: Holland, H.D., Turekian, K.K. (Eds.) *Treatise on Geochemistry*. Second Edition, Elsevier, Amsterdam, 1–39 https://doi.org/10.1016/B978-0-08-095975-7.00201-1

Patino, L.C., Carr, M.J., Feigenson, M.D. (2000) Local and regional variations in Central American arc lavas controlled by variations in subducted sediment input. *Contributions to Mineralogy and Petrology* 138, 265–283. https://doi.org/10.1007/s004100050562

Peterson, M.E., Saal, A.E., Nakamura, E., Kitagawa, H., Kurz, M.D., Koleszar, A.M. (2014) Origin of the 'Ghost Plagioclase' Signature in Galapagos Melt Inclusions: New Evidence from Pb Isotopes. *Journal of Petrology* 55, 2193–2216. https://doi.org/10.1093/petrology/egu054

Peterson, M.E., Saal, A.E., Kurz, M.D., Hauri, E.H., Blusztajn, J.S., Harpp, K.S., Werner, R., Geist, D.J. (2017) Submarine Basaltic Glasses from the Galapagos Archipelago: Determining the Volatile Budget of the Mantle Plume. *Journal of Petrology* 58, 1419–1450. https://doi.org/10.1093/petrology/egx059

Plank, T., Langmuir, C.H. (1998) The chemical composition of subducting sediment and its consequences for the crust and mantle. *Chemical Geology* 145, 325–394. https://doi.org/10.1016/S0009-2541(97)00150-2

Salters, V.J.M., Stracke, A. (2004) Composition of the depleted mantle. *Geochemistry ,Geophysics, Geosystems* 5, Q05B07. https://doi.org/10.1029/2003GC000597

Stubbs, D., Yang, R., Coath, C.D., John, T., Elliott, T. (2022) Tungsten isotopic fractionation at the Mariana arc and constraints on the redox conditions of subduction zone fluids. *Geochimica et Cosmochimica Acta* 334, 135–154. https://doi.org/10.1016/j.gca.2022.08.005

Tappe, S., Budde, G., Stracke, A., Wilson, A., Kleine, T. (2020) The tungsten-182 record of kimberlites above the African superplume : Exploring links to the core-mantle boundary. *Earth and Planetary Science Letters* 547, 116473. https://doi.org/10.1016/j.epsl.2020.116473

Tusch, J., Sprung, P., van de Löcht, J., Hoffmann, J.E., Boyd, A.J., Rosing, M.T., Münker, C. (2019) Uniform ^{182}W isotope compositions in Eoarchean rocks from the Isua region, SW Greenland: The role of early silicate differentiation and missing late veneer. *Geochimica et Cosmochimica Acta* 257, 284–310. https://doi.org/10.1016/j.gca.2019.05.012

Tusch, J., Hoffmann, J.E., Hasenstab, E., Fischer-Gödde, M., Marien, C.S., Wilson, A.H., Münker, C. (2022) Long-term preservation of Hadean protocrust in Earth's mantle. *Proceedings of the National Academy of Sciences* 119, e2120241119. https://doi.org/10.1073/pnas.2120241119

Völkening, J., Köppe, M., Heumann, K.G. (1991) Tungsten isotope ratio determinations by negative thermal ionization mass spectrometry. *International Journal of Mass Spectrometry and Ion Processes* 107, 361–368. https://doi.org/10.1016/0168-1176(91)80070-4

Wegner, W., Wörner, G., Harmon, R.S., Jicha, B.R. (2011) Magmatic history and evolution of the Central American Land Bridge in Panama since Cretaceous times. *Bulletin of the Geological Society of America* 123, 703–724. https://doi.org/10.1130/B30109.1

Werner, R., Hoernle, K., Barckhausen, U., Hauff, F. (2003) Geodynamic evolution of the Galápagos hot spot system (Central East Pacific) over the past 20 m.y.: Constraints from morphology, geochemistry, and magnetic anomalies. *Geochemistry, Geophysics, Geosystems* 4, 1108. https://doi.org/10.1029/2003GC000576

White, W.M., McBirney, A.R., Duncan, R.A. (1993) Petrology and geochemistry of the Galápagos Islands: Portrait of a pathological mantle plume. *Journal of Geophysical Research: Solid Earth* 98, 19533–19563. https://doi.org/10.1029/93JB02018

Willbold, M., Elliott, T., Moorbath, S. (2011) The tungsten isotopic composition of the Earth's mantle before the terminal bombardment. *Nature* 477, 195–198. https://doi.org/10.1038/nature10399

Wörner, G., Harmon, R.S., Wegner, W. (2009) Geochemical evolution of igneous rocks and changing magma sources during the formation and closure of the Central American land bridge of Panama. In: Kay, S.M., Ramos, V.A., Dickinson, W.R. (Eds.) *Backbone of the Americas: Shallow Subduction, Plateau Uplift, and Ridge and Terrane Collision.* GSA Memoir 204, Geological Society of America, Boulder, 183–196. https://doi.org/10.1130/2009.1204(08)